Insights into the formation mechanism of hard sludge on the secondary side of PWR steam generators

Kevin Beal, Lisa Million-Picallion, Sophie Delaunay, Gilles Berger, Grégory Lefèvre

Insights into the formation mechanism of hard sludge on the secondary side of PWR steam generators

K. Beal[1, 2], L. Million-Picallion[3], S. Delaunay[1], G. Berger[3], G. Lefèvre[2]

[1] EDF, R&D/Chemistry and Corrosion Group, Av. des Renardieres, 77818 Moret-sur-Loing, France

[2] PSL Research University, Chimie ParisTech - CNRS, 75005, Paris, France

[3] IRAP, CNRS- Université Paul Sabatier, 14 Av. Edouard Belin, 31400 Toulouse, France

Abstract

In the secondary circuit of nuclear Pressurized Water Reactors, corrosion products and impurities lead to the formation of undesirable hard deposits, called hard sludge, on the tube sheet of steam generators. Theses deposits are mainly composed of iron (magnetite), alumina and silica. The formation of hard sludge piles is investigated by reproducing the reaction of precursor oxides in the conditions of the steam generator (275°C, 58 bar). Mixtures of magnetite, γ-alumina and amorphous silica in binary or ternary systems in an alkaline ethanolamine-ammonia solution at pH25°C = 9.6 are studied. Carbon steel was tested as an alternative source of iron.

The analysis of the evolution of the suspensions, completed by the industrial feedback, allows to explain the process of hard sludge formation in the steam generators. The following sequence is proposed: sedimentation of magnetite / confinement of the interstitial fluid / concentration of aqueous species such as aqueous silica and alumina / sorption of Al on magnetite and/or growth of boehmite / reaction with aqueous silica to form kaolinite as a resistant cement. Once formed, the kaolinite cement tends to densify over time while magnetite is passive. The absence of Fe-

phyllosilicates predicted by thermodynamics is explained by the low solubility of magnetite making unfavorable the precipitation of Fe-silicate.

By contrast, metallic iron is not stable at contact with water and the continual production of divalent iron, whose solubility is much higher than that of magnetite, allows to overpass a threshold concentration what makes possible the precipitation of a berthierine layer at the surface of corroded steel. This layer constitutes the nucleation site for the further precipitation of other aluminosilicates.

Keywords: alumino-silicates ; thermodynamic modelling ; phase characterization ; hydrothermal reactions

1. Introduction

The hydrothermal crystallization of silicates phases in the Si-Al-Fe system may lead to industrial constraints that can be encountered in the nuclear industry in at least two contexts: the geological repository for nuclear wastes and the formation of hard sludges in the steam generator of the Pressurized Water Reactors (PWR) nuclear plants. In the first situation, the chemical reactions between the Fe-canister and the surrounding clays have been extensively studied in laboratory [1] [2] [3] [4] [5] [6] [7] and pilot experiments [8]. By contrast, the formation of deposits with this composition in the steam generators of PWR plants, called hard sludges, is a newer and less studied issue that can affect the reactor performance.

In the secondary circuit of nuclear Pressurized Water Reactors, corrosion products and impurities lead to the formation of hard deposits on the tube sheet of steam generators (SG). These deposits could lead to SG tubes denting, or a local increase of temperature, which could then promote stress corrosion cracking of SG tubes [9]. Although magnetite is the main compound, high impurities concentrations, in particular aluminum and silicon oxides, are found in hard sludge compositions [10] [11]. Mechanisms that lead to the formation and consolidation of hard sludge have not been identified [12]. Analysis of sludge pile deposits from plants suggests that the impurities may have a significant role in their formation [13]. Some studies [14] [15] have also reported that minor impurities, such as calcium and zinc, can be involved in deposits consolidation mechanisms by forming new phases such as willemite (Zn_2SiO_4) or calcium sulfate.

Despite their complex structure and composition, a simplified model of hard sludge may be proposed: an aluminosilicate matrix containing the magnetite particles. This simplified model constituted the frame of our study. A previous experimental study [16] [17] focused on the first stage of hard sludge formation: the sorption of aqueous aluminum or boehmite precipitation at the surface of magnetite particles acting as nucleation sites for the further growth of silicate. The aim of this experimental study focuses on the second stage of the process: the conversion of precursor

(magnetite (Fe_3O_4), alumina ($\gamma-Al_2O_3$), silica (SiO_2)) into consolidated hard sludge, and to better understand the formation mechanisms and the role of the different parameters (chemical species and time).

We lead to react at 275°C assemblages of alumina, silica and magnetite, as well as binary systems, in an alkaline solution modeling the secondary circuit fluid. The mineral transformation was characterized after one to few weeks of reaction by appropriate technics and compared to thermodynamic predictions. We also tested carbon steel as an alternative source of iron.

2. Materials and methods

In steam generators, sedimentation on the top of the tube sheet creates a confined media where the fluid circulation is minimal and where impurities may reach higher concentrations leading to the formation of new mineral phases. We experimented this confined media by using a hydrothermal reactor used in a static closed system. In addition to magnetite, the impurities were introduced in the system in the form of oxides powder, i.e. γ–alumina ($\gamma-Al_2O_3$) for aluminium and amorphous silica (SiO_2) for silicon.

2.1. Experimental facility

The experimental device (Figure 1) is based on a 450 mL commercial reactor (Parr Instrument©) made of pure titanium (grade 4) and used in a static mode, where the system remains closed during tests, without flow of the solution. The internal volume of the vessel is stirred by an impeller (around 200 rpm), driven by an external magnetic driver, and the temperature is controlled with an immersed thermocouple. This device is connected to a back-pressure regulator.

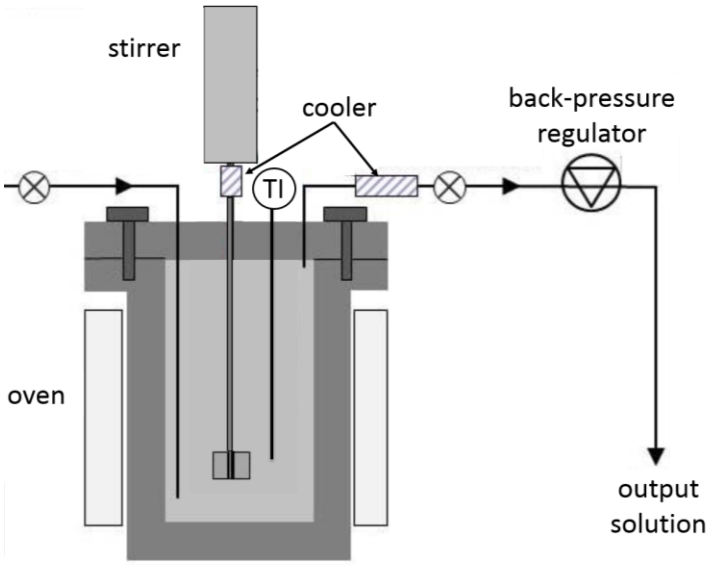

84

85 *Figure 1. Scheme of the experimental design*

86

87 *2.2. Test conditions*

88 The static experiments presented here were conducted at 275°C under vapor pressure, i.e. 58 bar.
89 PWR secondary circuit chemistry is reproduced using an alkaline solution at pH(25°C) = 9.6 containing
90 3 ppm concentration of ethanolamine and 1 ppm of ammonia. 1 ppm of N_2H_4 was added to remove
91 the remaining trace of oxygen but it decomposed quickly during the heating.

92 Several parameters were continuously monitored, as pressure, temperature and stirring rate. A
93 solution sample was regularly withdrawn (around 6 samples during an experiment) to measure the
94 pH and the concentration of amines and mineral species. The followed protocol was (1) stopping the
95 stirring to allow particles to settle, (2) withdrawing the cooled solution, (3) filtering it (filter 0.2 µm).

96 Proportions of oxides were calculated according to hard deposits compositions removed from
97 steam generators of several countries [10]. Tests were first performed with the three simultaneous
98 oxide additions at several different times. Table 1 summarizes all these tests conditions.

99

Table 1. Composition of the reacted the ternary oxide mixture

Element	Solid	Concentration of solids (g/L)	%w of solids	Concentration in elements (mM)
Fe	Magnetite	10	62	43
Al	γ-alumina	3.9	24	38
Si	Silica	2.2	14	37

In addition to these reference experiments, binary systems using alumina + magnetite, alumina + silica or silica + magnetite were experimented. We also conducted runs using carbon steel (metallic iron) as the source of iron instead of magnetite. Table 2 summarizes this second set of experiments.

Table 2. Experimental conditions

Solids	Time at 275°C
Magnetite + silica + alumina	7 days
	18 days
	30 days
	180 days
Magnetite + alumina	30 days
Alumina + silica	
Magnetite + silica	
Carbon steel + alumina + silica	

2.3. Chemicals

γ–alumina is provided by Merck© under the reference 01095 (purity > 99.5%). The magnetite and amorphous silica samples are high purity chemicals commercialized by Alfa Aesar© (ref. 12962 and

89709, respectively). X-Ray diffractograms and microscopic observations of the starting reactants are shown in Figure 2. The magnetite sample shows few % of hematite impurity.

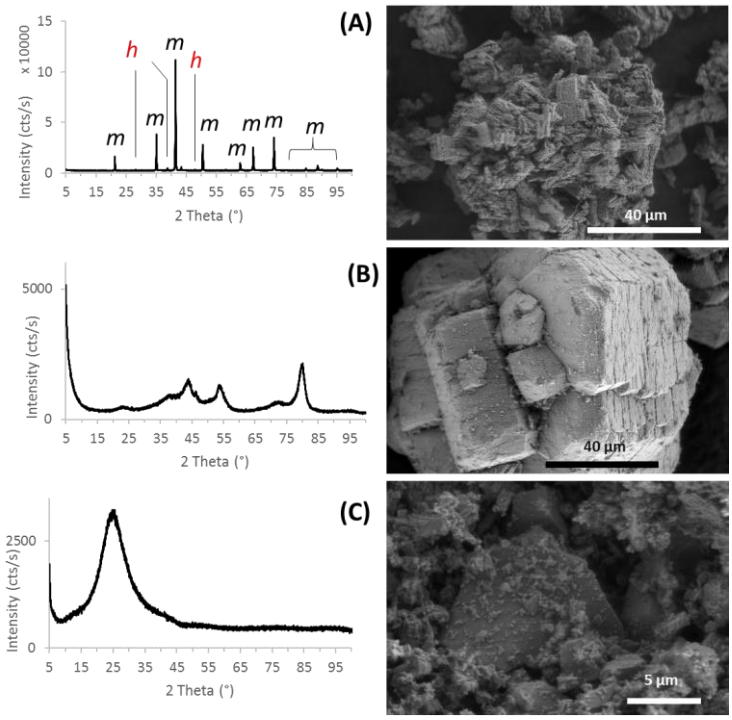

Figure 2: Diffraction patterns (left) and microscopic observations (right) of the starting reactants: (A) magnetite (diffraction peaks of magnetite and hematite are indicated by m and h, respectively), (B) alumina, (C) silica.

The composition of the carbon steel used in the second set of experiments is reported in Table 3.

Table 3. Minor elements content in 18MNDS steel

Element	Al	C	Co	Cr	Mn			
%w	0.024	0.199	0.01	0.19	1.56			
	Mo	N	Nb	Ni	P	S	Si	Ti
	0.53	0.0036	0.01	0.64	0.002	0.001	0.22	0.01

2.4. Characterizations

The morphology of the film surface was imaged with a high-resolution Sigma Zeiss scanning electron microscope (SEM) at an acceleration voltage between 5 and 10 kV, and additional characterizations of the film surface were conducted using secondary electron imaging and energy-dispersive X-ray spectrometry (EDX). The crystallographic structure of the film was characterized by X-ray diffraction (XRD) using a Rigaku Geigerflex with a Co anode, or a Brucker D8 Discover with a Cu anode. µRaman spectroscopy has been performed using a Renishaw InVia Reflex with a 532 nm laser.

One sample has been analyzed using a transmission electron miscroscope (MET) OSIRIS 200kV after its preparation using a focused electron beam in Scanning Transmission Electron Microscopy High-Angle Annular Dark-Field (STEM HAADF) mode.

Solutions have been analyzed with an Inductive Coupled Plasma – Atomic Emission Spectroscopy (ICP-AES) ThermoFischer iCAP 6500.

2.5. Numerical modeling

Speciation calculations of the solid-solution systems investigated have been performed using the software CHESS [18], a geochemical simulator developed to simulate the water-mineral interactions. The associated database included in the software package was completed with data coming from MulteQ database, an improved database developed by Electric Power Research Institute to address high temperature chemistry, especially in cooling circuits of PWR.

3. Results

Sampling aliquots of solution during the course of the experiments allowed to monitor changes in the fluid chemistry with time. The aqueous concentration of Si and Al increased and remained in the 100-200 ppm range for silica and 2-4 ppm range for alumina from ca. 180h. The pH decreased of 1

unit, in agreement with calculations indicating that it is due to the formation of negatively charged silica species. The main effort concerns the characterization of the mineral by-products. We first present the Si-Fe-Al system that is representative to the industrial environment. In a second stage, we will explore binary subsystems and an alternative source of iron in order to better discuss the results of the reference system.

3.1. Ternary system (magnetite+alumina+silica)

After a 7-day ageing period, the mixture of magnetite-alumina-silica has been observed by SEM-EDX (Fig. 3). The sample consists of particles of about 10µm sized, with the same microporosity as the magnetite added in the reactor. The EDX analysis confirms the composition (only Fe and O). On the other hand, it can be observed that both aluminum and silica are accumulated on the edges of the magnetite particles.

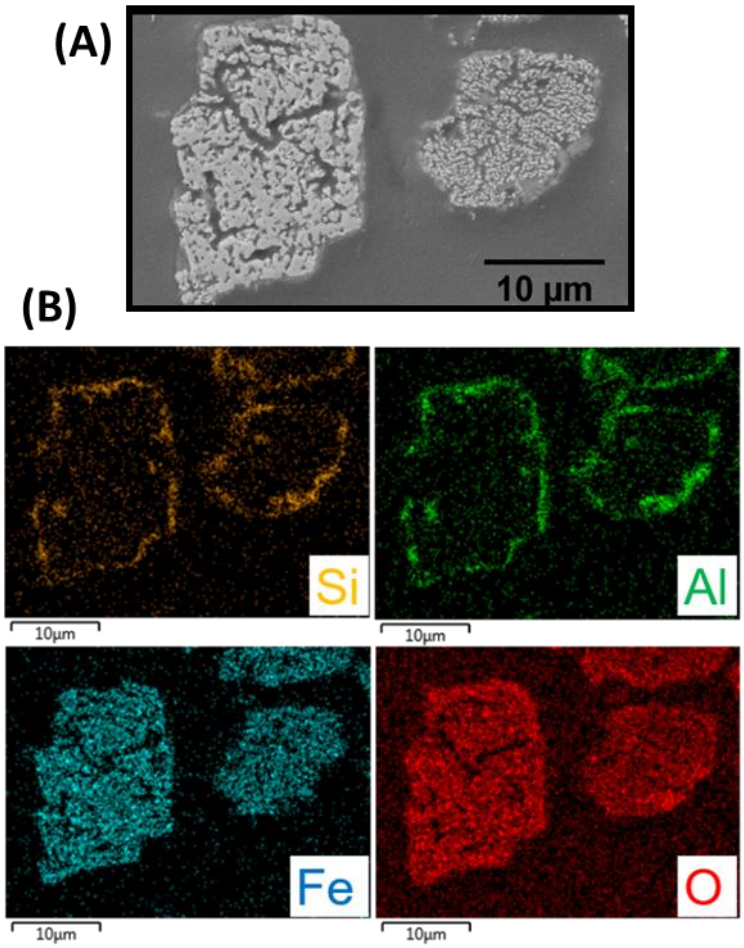

Figure 3. Pictures of sample cross-section after a 7-day ageing period: (A) secondary electron SEM, picture and (B) EDX mapping for the four elements indicated.

The diffractogram of this sample (Fig. 4) is dominated by the peaks of magnetite (with some impurities of hematite whose content seems constant), with the presence of kaolinite ($Al_2Si_2O_5(OH)_4$) and boehmite (γ-AlO(OH)). This latter phase is expected, due to the hydration of γ-alumina in hydrothermal conditions [19], while kaolinite comes from the reaction between silica and γ-alumina. The molar ratio of Al/Si in the system is around 1, as in the formula of kaolinite, so boehmite is not formed due to an excess of aluminum.

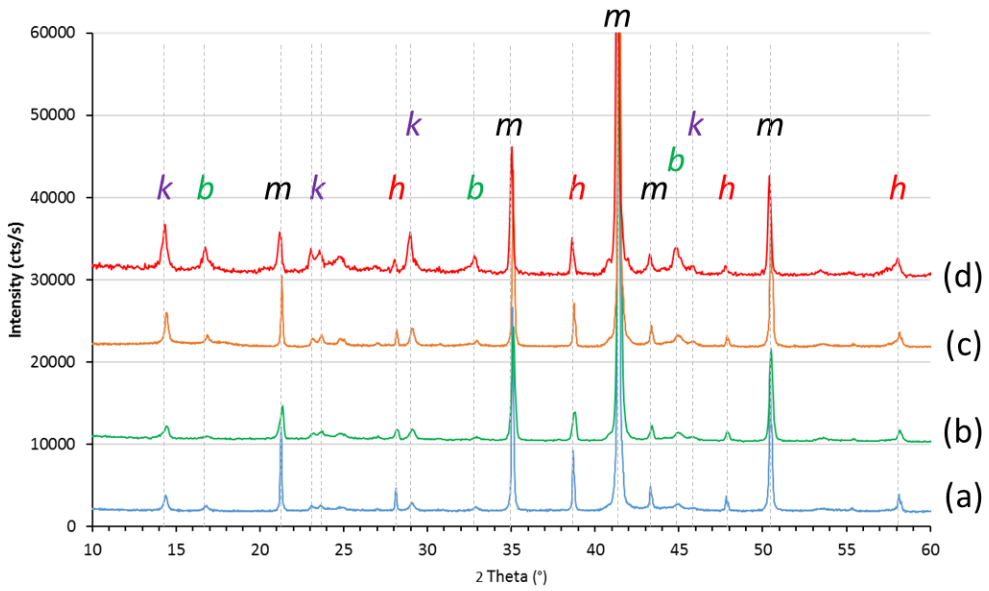

Figure 4. XRD analysis of samples as a function of ageing, after (a) 7 days, (b) 18 days, (c) 30 days and (d) 180 days. The peaks identified for magnetite (m), hematite (h), kaolinite (k) and boehmite (b) are detailed.

176 The pictures in Fig. 5 show samples after different ageing periods. While the SEM picture after a
177 7-day ageing period showed no evolution compared to pristine magnetite, the pictures show a
178 growth of the size of the particles, with the formation of millimetric agglomerates.

179

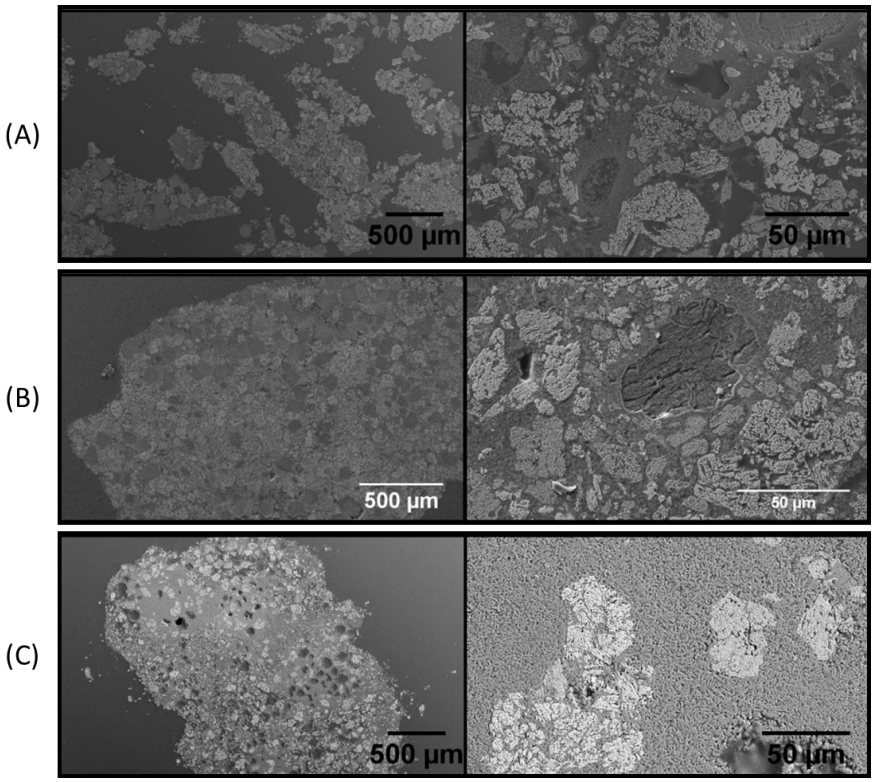

180

181 *Figure 5. SEM picture of samples cross-sections after different ageing periods: (A) 18 days, (B) 30 days*
182 *and (C) 180 days.*

183

184 In the diffractograms (Fig. 4), the peaks corresponding to kaolinite and boehmite increase, to
185 reach a maximum at 180 days. A detailed analysis for 30-day ageing is presented in Figure 6. EDX
186 maps in Fig. 6C shows several phases: magnetite particles remain free of Si and Al, and looks like the
187 pristine solid, and some particles of γ-alumina are visible. However, no particle of silica has been
188 identified (which would correspond to a zone in EDX map free of Al and Fe), but on the contrary, Si is
189 systematically associated with Al and is present around each particle of magnetite or γ-alumina. This

picture shows undoubtedly that an aluminosilicate plays the role of cement to consolidate the sample initially consisting in dispersed particles in suspension.

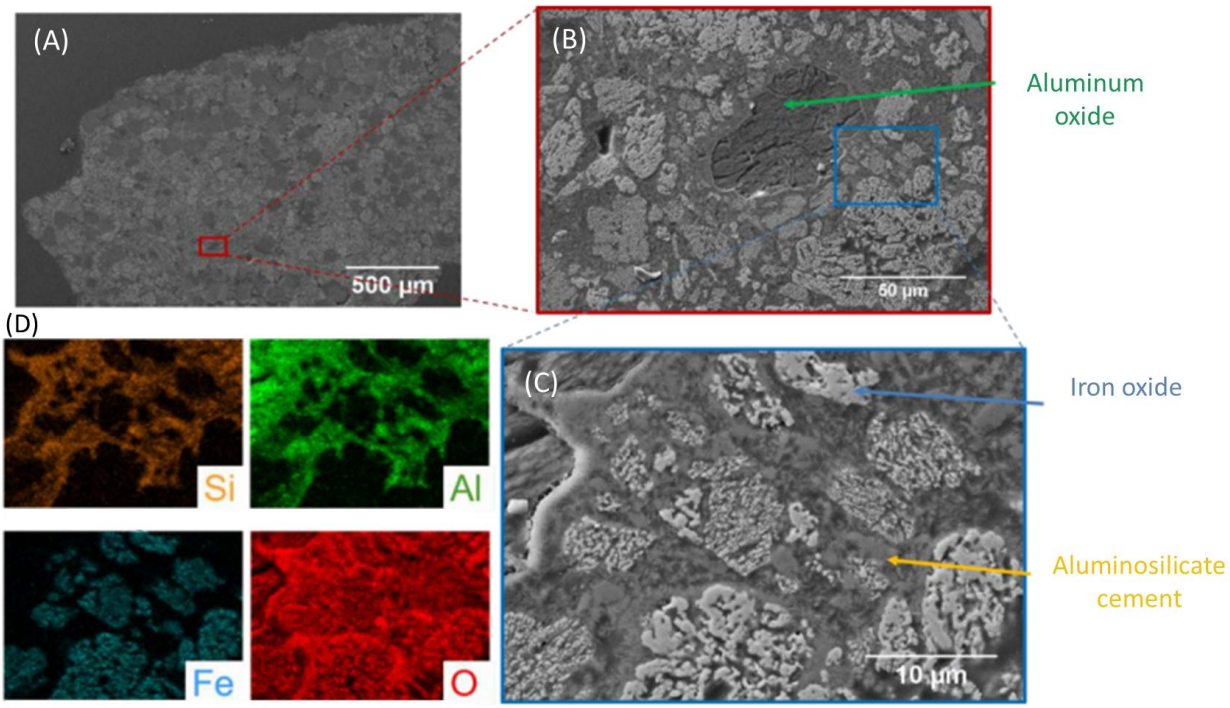

Figure 6. Cross-section of sample after 30-day ageing: (A) to (C) SEM with increasing magnification, and (D) EDX map of (C) picture.

To go further in the understanding of the structure of the sample, its surface has been observed by SEM (Fig. 6). It was found to be covered by layers, whose geometry is typical of clays. The MET STEM HAADF (Fig. 7) shows the cross section of these layers, stacked in a non-compact way. On the contrary, in the vicinity of the magnetite particles, a dense zone is observed where the layers look oriented parallel to the surface of the particles, and seem to have merged. The cement observed in previous figures is present in two distinct forms: the denser zone would result from a growth of the clay at the surface of the magnetite, while the non-compact zone would result from the agglomeration of precipitated layers, due to settling or electrostatic interactions.

205 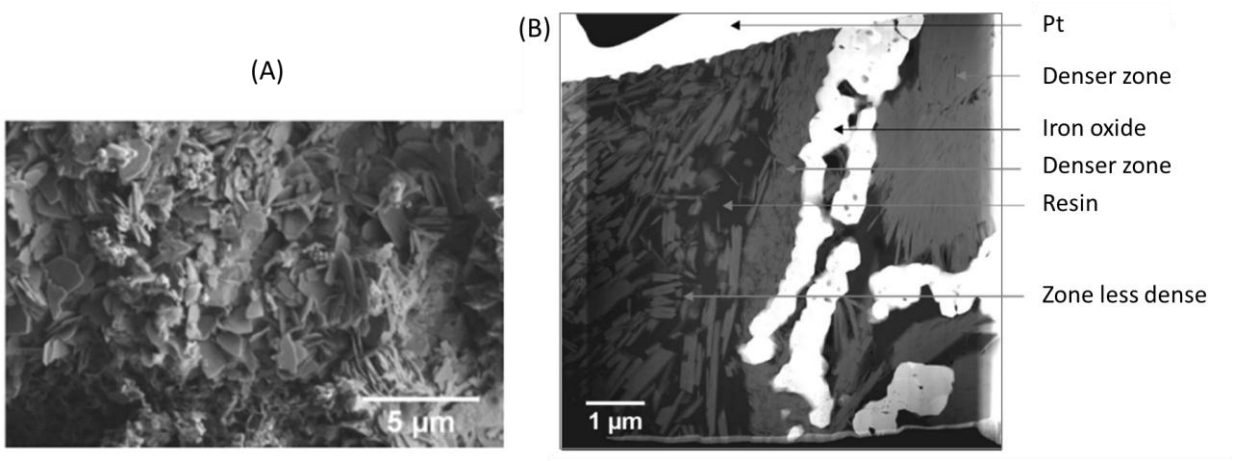

206 *Figure 7. Sample after 30-day ageing: (A) SEM and (B) STEM HAADF*

207

208 *3.2. Binary systems*

209 The previous experiments have shown that the reason of the consolidation is the formation of a
210 cement consisting in kaolinite. Binary systems have been experimented to evaluate the specific role
211 of Al and Si. It could also bring interesting results on the consolidation in the case of a Si/Al ratio far
212 from 1, which is possible in steam generators.

213 In Figure 8 we reported the SEM-EDX observations relative to the three binary systems. In
214 absence of magnetite, the sample consists in alumina particles (on the right of the Fig. 6B) mixed
215 with kaolinite (on the left). XRD analysis (not shown) reveals only boehmite and kaolinite. It can be
216 concluded that magnetite is not needed to trigger the formation of kaolinite, what is consistent with
217 the kaolinite layers found far from its surface (Fig. 6). In the magnetite-alumina system, boehmite
218 and diaspore have been identified by XRD. The SEM-EDX analysis shows the precipitation of
219 aluminium hydroxide (identified as diaspore by µRaman) in the porosity of magnetite particles with a
220 low amount of aluminium at the external surface of magnetite. Moreover, no consolidation has been
221 observed, which indicates that the aluminium hydroxide is not able to play the role of cement
222 between magnetite particles. However, its high affinity towards this iron oxide is demonstrated, and
223 this surface accumulation of aluminium would allow the growth of kaolinite on its surface. In the

magnetite-silica system, some consolidation is locally observed, and the SEM-EDX show opposite maps for Si and Fe. The magnetite particles are embedded in a silica gel coming from the dissolution of silica particles. No crystalline phase except iron oxides is detected in diffractogram.

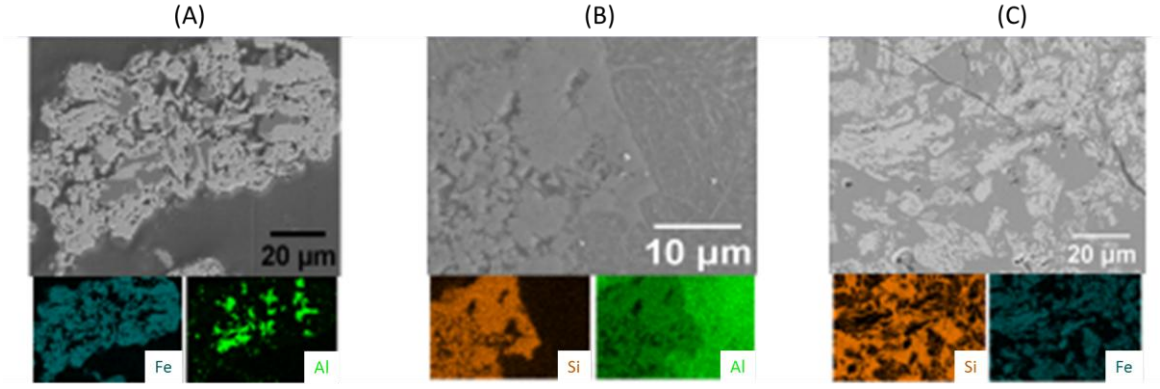

Figure 8. SEM pictures and EDX map of binary systems: (A) magnetite-alumina, (B) silica-alumina, (C) magnetite-silica.

3.3. Role of metallic iron

From the previous experiments, the magnetite seems to have no role in the chemical reaction in the system. Its solubility should be too low, as well as its dissolution kinetics, to release enough soluble iron. In the secondary circuit, iron is present as magnetite, but large parts of the circuits are made in carbon steel, which is subject to severe corrosion. As observed in literature at lower temperature, this could change the iron reactivity.

To evaluate the impact of the iron availability, another experiment has been done with a carbon steel coupon inside a suspension of alumina and silica. The SEM pictures and EDX maps of the cross section of the coupon are shown in Figure 9. Contrary to the experiments with magnetite, in the XRD analysis, the presence of berthierine ($Fe_2Al_2Si_2O_5(OH)_4$) has been detected. The cross section shows

(from left to right) the carbon steel covered by the native corrosion layer, then a thick layer of Fe-Al-Si oxide (berthierine), and a thin layer of aluminosilicate covered by the resin.

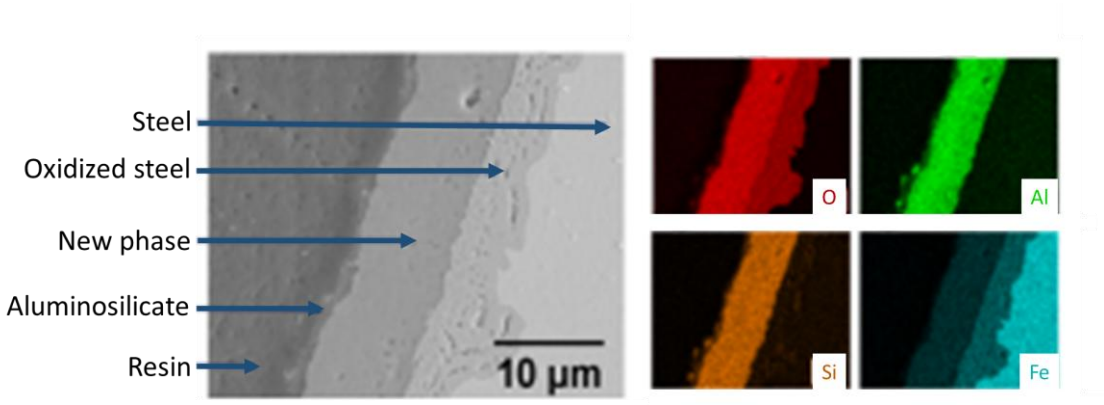

Figure 9. SEM pictures and EDX maps of a cross section of carbon steel/alumina/silica system

This observation is a proof that the oxidation of carbon steel release iron ions, which react with dissolved silica and aluminum, or with the aluminosilicate layer already present at the interface to form berthierine.

4. Discussion

Thermodynamic calculations have been made to simulate the evolution of the system consisting in the mixture of magnetite, γ-alumina and amorphous silica. We did not consider the precipitation of unlikely phases at this temperature such as corundum (α-Al_2O_3) that is supposed to not occur for kinetic reasons. In the absence of silica, the only predicted reaction is the recrystallization of alumina in stable hydroxides. In absence of magnetite, alumina and silica feed the precipitation of kaolinite or its polymorph (dickite). In the absence of alumina, Fe-silicates (cronstedtite and Fe-serpentine) constitute the stable secondary phases. In the ternary system, the calculations predict the formation of iron phyllosilicates at the expense of the starting oxides. Figure 10 summarizes the diversity of predicted stable parageneses depending on the starting oxides considered.

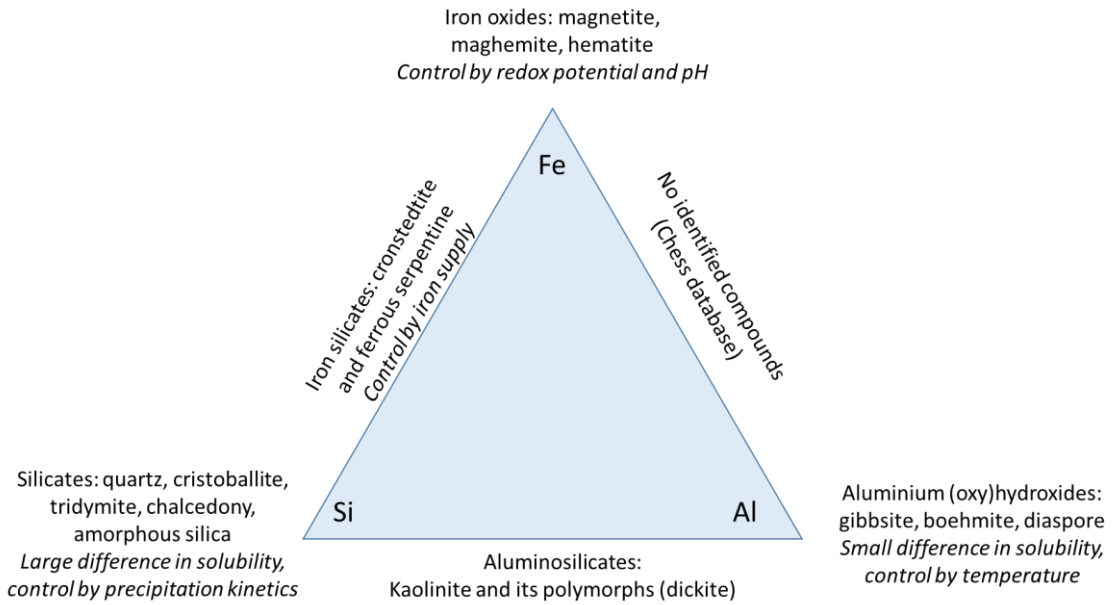

Figure 10: Predicted stable phases in the system Al_2O_3-SiO_2-Fe_3O_4

The conclusions based on Fig. 9 are well known by the geochemist in the Earth sciences. For example, the mineral "Chamosite-7Å" predicted in the ternary system is a proxy for berthierine, a 1:1-type layer silicate [20]. It was previously recognized (both theoretically and experimentally listed in the introduction) in investigations on underground storage of nuclear wastes, as the results of the interaction of metallic iron (waste container) and the clayed barrier (bentonite). From these studies, and our own simulations, the formation of berthierine or another iron phyllosilicate was expected in our ternary reference system, but it was not observed. By contrast, when using carbon steel as the source of iron the observation is consistent with the thermodynamic prediction. This discrepancy may be attributed to the low solubility of magnetite (the Fe source in our reference experiments). Indeed, the mineral reactions proceed by combination of aqueous species for nucleation and growth and at very low concentration of aqueous iron the precipitation of Fe-silicates is very slow, and these phases are improbable. In the presence of unstable metallic iron, the dissolution of iron, in true aqueous species or as colloids, is significant enough and does not limit the Fe-silicate growth.

Thus, the hard sludge environment is better modeled by a binary alumina-silica, magnetite being inert. The following general sequence of reaction can be proposed: sedimentation of magnetite => confinement of the interstitial fluid => concentration of aqueous species such as aqueous silica and alumina => sorption of Al on magnetite and/or growth of boehmite => reaction with aqueous silica to form kaolinite. It is noticeable that kaolinite, a cl mineral, may form a resistant cement at the microscopic scale.

In the presence of steel corrosion, the reaction is radically different. Metallic iron is not stable at contact with water and the continual production of divalent iron, whose solubility is much higher than that of magnetite, allows to overpass a threshold concentration what makes possible the precipitation of berthierine. The berthierine precipitation at the contact of the corroded metal constitutes the nucleation site for other aluminosilicate and is so the sink of silica. This affinity of silica for corroded steel can be viewed as a competitive process of the hard sludge formation and we can even speculate that, from this point of view, the corrosion of steel may potentially prevent the formation of hard sludge.

5. Conclusion

Based on the industrial feedback and the laboratory works that has allowed the identification of phenomena of agglomerations, this study aimed to identify and understand the mechanisms of formation of hard sludge. The analysis of the suspension behavior and the decorrelation of the parameters have generated a large number of information to explain the origins of the phenomenon of agglomeration, which can be linked to the formation of hard sludge in the steam generators.

The analysis, correlation and comparison of these results allow not only to clearly identify this phenomenon of agglomeration but also to deduce the mechanism. The in-depth analyses of the samples have shown that the agglomeration of the powders is the consequence of the formation of a cement that binds and traps the particles. This cement has been identified as being exclusively

304 kaolinite when magnetite is the iron-bearing solid. This cement is denser towards the surface of the
305 particles it traps. The orientation of kaolinite crystals suggests that part of the cement is formed on
306 the surface of the particles (magnetite and boehmite) by crystal growth, while the other, less dense,
307 part is formed by sedimentation and/or coagulation of kaolinite. Once formed, the kaolinite cement
308 tends to densify over time. Although this kaolinite cement is dependent on the presence of
309 aluminum and silicon, it is independent of the presence of magnetite. Furthermore, the experiments
310 have shown that if they do not react together to form an aluminosilicate, these two species may still
311 contribute to the densification of deposits. In the case of aluminum, by filling the porosities of the
312 magnetite in forming diaspore, and, in the case of silicon, by forming a compact gel around the
313 particles of magnetite. In addition to the identification of phases favoring agglomeration, the growth
314 of hydroxide of aluminum on the surface of the magnetite highlights the reactivity of aluminum
315 versus magnetite. Whereas magnetite seems inert to cement, it is not inert towards aluminum,
316 which once on the surface of the magnetite, can be a growth site for kaolinite cement.

References

[1] B. Lanson, S. Lantenois, P. A. van Aken, A. Bauer et A. Plançon, «Experimental investigation of smectite interaction with metal iron at 80 °C: Structural characterization of newly formed Fe-rich phyllosilicates,» *American Mineralogist,* vol. 97, pp. 864-871, 2012.

[2] S. Lantenois, B. Lanson, F. Muller, A. Bauer, M. Jullien et A. Plançon, «Experimental Study of Smectite Interaction with Metal Fe at Low Temperature: 1. Smectite Destabilization,» *Clays and Clay Minerals,* vol. 53, pp. 597-612, 2005.

[3] R. Mosser-Ruck, M. Cathelineau, D. Guillaume, D. Charpentier, D. Rousset, O. Barres et N. Michau, «Effects of Temperature, pH, and Iron/Clay and Liquid/Clay Ratios on Experimental Conversion of Dioctahedral Smectite to Berthierine, Chlorite, Vermiculite, or Saponite,» *Clays and Clay Minerals,* vol. 58, pp. 280-291, 2010.

[4] M. Perronnet, M. Jullien, F. Villiéras, J. Raynal, D. Bonnin et G. Bruno, «Evidence of a critical content in Fe(0) on FoCa7 bentonite reactivity at 80 °C,» *Applied Clay Science,* vol. 38, pp. 187-202, 2008.

[5] M. Osacky, V. Sucha, A. Czimerova et J. Madejov, «Reaction of smectites with iron in a nitrogen atmosphere at 75 °C,» *Applied Clay Science,* vol. 50, pp. 237-244, 2010.

[6] S. Kaufhold, A. Hassel, D. Sanders et R. Dohrmann, «Corrosion of high-level radioactive waste iron-canisters in contact with bentonite,» *Journal oh Hazardous Materials ,* vol. 285, pp. 464-473, 2015.

[7] C. Rivard, M. Pelletier, N. Michau, A. Razafitianamaharavo, I. Bihannic, M. Abdelmoula, J. Ghanbaja et F. Villiéras, «Berthierine-like mineral formation and stability during the interaction of kaolinite with metallic iron at 90 C under anoxic and oxic conditions,» *American Mineralogist,* vol. 98, pp. 163-180, 2013.

[8] P. D. Svensson et S. Hansen, «Redox Chemistry in Two Iron-Bentonite Field Experiments at Äspö Hard Rock Laboratory, Sweden: An XRD and Fe K-Edge XANES Study,» *Clay and Clays Minerals,* vol. 61, pp. 566-579, 2013.

[9] R. Wolfe et H. Feldman, «Steam generator management program: PWR steam generator top-of-tubesheet denting,» EPRI Rep., no. 3002002197, 2014.

[10] H. Feldman, «Steam generator management program: assessment of the effect of deposit removal frequency on sludge management,» EPRI Rep. 1025127, 2012.

[11] R. Fernandez-Saavedra, M. Gomez-Mancebo, M. Fernandez-Dias et D. Gomez-Briceno, «Role of aluminum and silicon species in the formation of hard sludge on the secondary side of PWR steam generators: Potential geopolymers contribution,» *Progress in Nuclear Energy,* vol. 118, p. 103136, 2020.

[12] M. Vepsäläinen, «Deposit formation in PWR steam generators,» Research report VTT (VTT-R-

00135-10), 2010.

[13] T. Dorsch, «Chemo-physical characterization on steam generator hard sludge particles,» AREVA Technical Rep. PTCC-G/2014/en/0081, 2014.

[14] C. Turner, «Factors affecting the consolidation of steam generator sludge,» AECL report (AECL-10759), 1993.

[15] C. Turner, «Physical and chemical factors affecting sludge consolidation,» AECL Technical Report (AECL611674), 1997.

[16] L. Million-Picaillon, «Interactions magnétite-Al(III)-silice dans les conditions physico-chimiques des générateurs de vapeur des centrales nucléaires,» PhD, University of Toulouse, 2014.

[17] K. Beal, L. Million-Picallion, G. Lefèvre, G. Berger, S. Delaunay, C. Goujon et J.-L. Bretelle, «Formation and Consolidation of Hard Sludge under Secondary Circuit Conditions,» chez *Nuclear Plant Chemistry Conference*, Brighton, 2016.

[18] J. Van der Lee et L. De Windt, «CHESS Tutorial and Cookbook. Updated for version 3.0. Users Manuals,» Ecole des Mines de Paris, Fontainebleau, France, 2002.

[19] E. Girel, A. Cabiac, A. Chaumonnot, M. Besson et A. Tuel, «Selective Carbon Deposition on gamma-Alumina Acid Sites: toward the Design of Catalyst Supports with Improved Hydrothermal Stability in Aqueous Media,» *ACS Applied Materials & Interfaces,* vol. 12, pp. 13558-13567, 2020.

[20] E. Hornibrook et F. Longstaffe, «Berthierine from the lower cretaceous clearwater formation, Alberta, Canada,» *Clays Clay Minerals,* vol. 44, pp. 1-21, 1996.

[21] R. Fernández-Saavedra, «Hard sludge and denting in the secondary side of PWR steam generators,» chez *Nuclear Plant Chemistry Conference*, Sapporo, 2014.

319

320

321

322